Analytic model for minority carrier effects in nanoscale Schottky contacts

Lifeng Hao[a] and P. A. Bennett
School of Materials, Arizona State University, Tempe, Arizona 85287, USA

(Received 12 March 2010; accepted 13 May 2010; published online 2 July 2010)

We present an analytic model for the current-voltage (I-V) behavior for a nanoscale Schottky contact, emphasizing the role of minority carriers. The minority carriers give rise to a surface recombination current that can strongly dominate the majority current flow throughout the bias range. The I-V curve for the surface recombination current shows a weak rectifying behavior, which could be misinterpreted as large variations of ideality factor and effective barrier height. The model calculations show a good match with experimental I-V curves for nanoscale $CoSi_2$ epitaxial islands on Si(111) and for direct scanning tunnel microscope tip point contacts, for a range of island size, doping type, and surface Fermi level. © *2010 American Institute of Physics*.
[doi:10.1063/1.3448231]

I. INTRODUCTION

The current-voltage (I-V) behavior of an "ideal" metal-semiconductor (M-S) contact is given by

$$I(V) = AA^*T^2 \exp\left(-\frac{q\Phi_B}{kT}\right)\left(\exp\frac{qV}{nkT} - 1\right), \quad (1)$$

where A is the contact area size, A^* is the Richardson constant, Φ_B is the Schottky barrier height, and n is the ideality factor.[1] Practical diodes generally follow this behavior closely, with n close to 1. On the other hand, several studies report that nanoscale M-S contacts on an extended surface (point contact geometry) exhibit very large deviations from Eq. (1), characterized by large shifts of Φ_B and $n \gg 1$.[2–4] This has been explained as arising from field concentration effects,[5,6] which tend to reduce the barrier width and cause enhanced tunnel current, or from electrostatic screening by a strongly pinned surrounding surface,[7] which tends to reduce the thermionic current. For very small contacts (~1 nm), there may also be a significant variation in the intrinsic barrier height.[8] These works refer only to majority current that crosses the M-S interface. We have recently shown that the minority current arising from surface recombination and generation (R-G) in a point contact geometry can be magnitudes larger than the majority current, and can dramatically affect the net I-V behavior of nanoscale M-S contacts.[9] In this paper, we develop analytic expressions for the minority current flow for a point contact geometry and show detailed comparisons with experimental measurements for nanoscale contacts on Si(111). This model gives new insight to the problem of nanoscale contacts to semiconductors, in general.

The paper is organized as follows: we begin with a brief discussion of the influence of the surrounding free surface, and qualitatively describe a minority carrier current caused by the surface R-G process. We develop an analytic expression for the surface R-G current by considering the majority and minority carrier distribution along the surface. The model results are compared with experimental data, using epitaxial $CoSi_2$ islands or a W scanning tunnel microscope (STM) tip as metal contacts to Si(111) in ultrahigh vacuum. These data show contact-area-size independence of the zero-bias conductance (for $A < 10^4$ nm^2), strong and abnormal surface-Fermi-level dependence of the zero-bias conductance and a soft reverse breakdown for p-type substrate. All these features are explained by the analytic model.

II. TRANSPORT MODEL

Figure 1(a) shows the geometry of an ideal nano-Schottky contact: a round metal contact with radius r_0, placed on a Si(111) substrate and surrounded by a free surface. In the model, the surface state is a key point and its influence is considered from the three aspects below. First, the surface states work as traps for majority carriers, causing a depletion layer and built-in electric field under the surface, which determines the surface potential at zero bias. With bias applied to the point contact, trapped carriers release or accu-

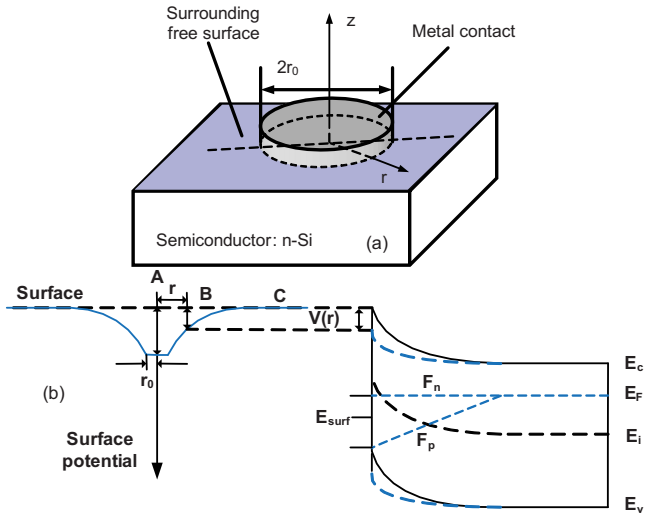

FIG. 1. (Color online) (a) Geometry of a nano-Schottky contact. (b) Surface potential under forward bias. (c) Band bending plots along z axis for positions B (dashed line) and C (solid line), near and far from the contact, as marked in (b). At C, the valence band edge is at the Schottky barrier height determined by the surface state and $E_{Fs}=E_{surf}$; while at B, the surface potential is lowered by the offset potential $V(r)$(see text for definition).

[a]Electronic mail: Lifeng.hao@asu.edu.

mulate, resulting in raising or lowering of the surface potential. We define $V(r)$ as the surface potential offset, corresponding to the surface potential deviation from its zero-bias (equilibrium) value. $V(r)$ drops to zero at infinity, as shown in Fig. 1(b). For simplicity, we show the case where the surface state far from the contact matches the metal Fermi level. Thus, for zero bias, the surface is in "flat-band" condition. This assumption is closely satisfied for $CoSi_2$ islands on Si(111). In the general case, these levels will not match, resulting in a local potential drop in a small region near the tip. This has a negligible effect on the total surface R-G current which is collected from a vast surface area, as we discuss later. Second, the surface states work as recombination centers to generate or annihilate electron-hole pairs when the carrier density at the surface deviates from the equilibrium value. Third, the built-in electric field keeps minority carriers near the surface, making the majority current and minority current spatially separated.

Combining the three effects above, we note that the surrounding free surface can provide a surface channel for minority carrier current via the surface R-G process. For example, under reverse bias, the surface potential is raised, resulting in generation of electron-hole pairs. The generated minority carriers go to the contact through the surface channel, while the generated majority carries are pushed out of the depletion region by the built-in field. Under forward bias, the minority carriers which are injected from the tip, travel in the surface channel and recombine with the majority carriers passing through the lowered surface Schottky barrier.

The total surface R-G current, $I_{\text{R-G}}$, is calculated by integrating the R-G current density over the active surface area, as

$$I_{\text{R-G}} = \int_{r_0}^{\infty} J_R(r) 2\pi r \mathrm{d}r, \tag{2}$$

where $J_R(r)$ is the recombination current density (A/cm^2) at position r, given by

$$J_R(r) = qR_s(r). \tag{3}$$

Here, $R_s(r)$ is the Schockley–Read–Hall R-G rate at position r, written as[10]

$$R_s(r) = \frac{\sigma_n \sigma_p v_{th} N_{it} [n_s(r) p_s(r) - n_i^2]}{\sigma_n [n_{1s} + n_s(r)] + \sigma_p [p_{1s} + p_s(r)]}, \tag{4}$$

in which $n_s(r)$ [or $p_s(r)$] is the electron (or hole) density at the surface, σ_n (or σ_p) is the electron (or hole) capture cross section of the R-G centers, v_{th} is thermal velocity given by $v_{th} = \sqrt{3kT/m}$, n_i is the density of electrons of intrinsic Si, and N_{it} is the surface density of the R-G centers. Here we have $n_{1s} = n_i \exp[(E_t - E_i)/kT]$ and $p_{1s} = n_i \exp[-(E_t - E_i)/kT]$, in which E_t is the surface state energy level for the R-G centers. For $\sigma_n = \sigma_p$, we have $E_t = E_i$ and hence $p_{1s} = n_{1s} = n_i$. This behavior is independent of the position of surface states in the band gap.[11] For $\sigma_n \neq \sigma_p$, the difference of cross sections causes a small shift in the energy level E_t from E_i to E_i^*,[12] given as

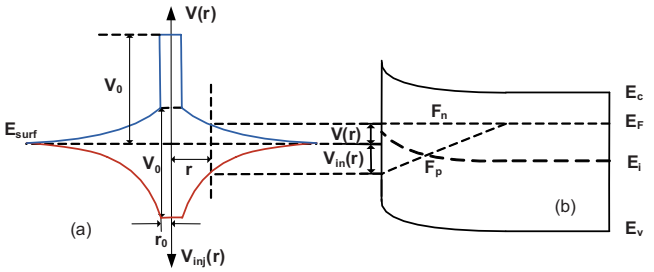

FIG. 2. (Color online) (a) Distribution of $V(r)$ and $V_{inj}(r)$ along surface. (b) Band bending diagram at position r.

$$E_i^* = E_i + \ln \frac{1}{\sqrt{\beta}}, \tag{5}$$

where $\beta = \sigma_n/\sigma_p$ is the ratio of the capture cross section of electrons to that of holes, so $n_{1s} = \sqrt{1/\beta} n_i$ and $p_{1s} = \sqrt{\beta} n_i$.

In Eq. (4), σ_n, σ_p, and N_{it} are determined by surface structures, so they can be regarded as constants. Thus, $R_s(r)$ and I simply depend on $n_s(r)$ and $p_s(r)$. To figure out $n_s(r)$ and $p_s(r)$, we assume the entire system is in steady state for all bias voltages. For simplicity, we consider n-type Si(111) under forward bias, but the arguments are easily extended to p-type and reverse bias.

A. Electron and hole concentration at the surface: $n_s(r)$ and $p_s(r)$

The surface concentrations $n_s(r)$ and $p_s(r)$ are determined by $F_{ns}(r)$ and $F_{ps}(r)$ separately as follows:

$$n_s(r) = n_i \exp \frac{F_{ns}(r) - E_i}{kT}, \tag{6}$$

$$p_s(r) = n_i \exp \frac{E_i - F_{ps}(r)}{kT}, \tag{7}$$

in which $F_{ns}(r)$ [$F_{ps}(r)$] is the electron (hole) quasi-Fermi level at the surface. Under zero-bias condition, we have $F_{ns}(r) = F_{ps}(r) = E_{Fs}$, in which E_{Fs} is the Fermi level at the surface under equilibrium. With bias, for majority carriers, $F_{ns}(r)$ always lines up with E_F, the Fermi level in the bulk, and rises by $V(r)$ in magnitude, as shown in Fig. 2(b), which is written as

$$F_{ns}(r) = E_{Fs} + qV(r). \tag{8}$$

The behavior of minority carriers $F_{ps}(r)$ is complicated. In a planar Schottky diode, $F_{ps}(r)$ is determined by the metal Fermi level. For the point contact, $F_{ps}(r)$ is not only determined by the energy level of the surface state, E_{surf}, which is equal to E_{Fs}, but also affected by the injection of minority carriers from the tip and their lateral movement along the surface. This causes an increase in minority carrier density at the surface and a shift in $F_{ps}(r)$ away from E_{Fs}, as shown in Fig. 2(b). We define

$$V_{inj}(r) = \frac{E_{Fs} - F_{ps}(r)}{q}, \tag{9}$$

which corresponds to the variation in the $F_{ps}(r)$ due to minority carrier injection. Substituting Eqs. (8) and (9) into Eqs. (6) and (7) separately, we have

$$n_s(r) = n_i \exp\frac{E_{Fs} - E_i + V(r)q}{kT}, \tag{10}$$

$$p_s(r) = n_i \exp\frac{-(E_{Fs} - E_i) + V_{inj}(r)q}{kT}. \tag{11}$$

Thus, $V(r)$ and $V_{inj}(r)$ determine $n_s(r)$ and $p_s(r)$ and hence the surface R-G current. For the free surface, we have $F_{ns}(r) - F_{ps}(r) = [V(r) + V_{inj}(r)]q$. At the boundary r_0, since both the lowering of the surface potential and the minority carrier injection are caused by the bias applied to the tip, we have

$$V(r_0) + V_{inj}(r_0) = V_0, \tag{12}$$

in which V_0 is the applied bias. At the metal side of the interface, we always have $V(r) = V_0$. Thus, $V(r)$ drops sharply, as shown in Fig. 2(a). The steep drop implies electric dipoles at the contact boundary, similar to the interface dipoles at a planar Schottky diode or at a pinned surface.[13] This assists minority carrier injection, since it lowers the lateral barrier seen by minority carriers. The magnitude of the steep drop at r_0 is equal to $V_{inj}(r_0)$ which determines the minority carrier injection level.

From the discussion above, we note that the majority and minority carrier flow may be treated separately, since one or the other strongly dominates in different regions. This is similar to the case for a planar p-n junction and makes it simple to derive $V(r)$ and $V_{inj}(r)$ expressions.

B. Majority carrier movement

The majority carriers (electrons) move from the bulk semiconductor to the surface in the form of thermionic emission current. Under steady state condition, all electrons that pass over the Schottky barrier and reach a certain position at the surface will annihilate there by the surface R-G process. This is because Si is a high mobility semiconductor and F_{ns} is always equal to E_F, as shown in Fig. 2(b). As a result, there is no lateral current of majority carriers. So we have

$$J_R(r) = J_{SB}(r), \tag{13}$$

in which $J_{SB}(r)$ is the thermionic emission current density at position r. Substituting Eqs. (1), (3), (4), (10), and (11) into Eq. (13), we get

$$\frac{q\sigma_n\sigma_p v_{th} N_{it} n_i^2 \left(\exp\frac{(V(r) + V_{inj}(r))q}{kT} - 1\right)}{\sigma_n\left(n_{1s} + n_i \exp\frac{E_{Fs} - E_i + V(r)q}{kT}\right) + \sigma_p\left(n_{1p} + n_i \exp\frac{-(E_{Fs} - E_i) + V_{inj}(r)q}{kT}\right)} = A^* T^2 \exp\left(\frac{-\Phi_B q}{kT}\right)\left[\exp\frac{V(r)q}{kT} - 1\right]. \tag{14}$$

The relationship of $V(r)$ and $V_{inj}(r)$, as shown in Eq. (14) is complex. To get a clear physical meaning, Eq. (14) can be simplified in the zero-bias region, defined by $V_0 q \ll kT$. Because $V(r) + V_{inj}(r) \leq V_0$, we have

$$\exp\frac{[V(r) + V_{inj}(r)]q}{kT} - 1 \approx \frac{[V(r) + V_{inj}(r)]q}{kT}, \tag{15}$$

$$\exp\frac{V(r)q}{kT} - 1 \approx \frac{V(r)q}{kT}. \tag{16}$$

We can choose V_0 small enough to fulfill $|E_{Fs} - E_i| \gg qV_0$, and we have

$$\exp\frac{E_{Fs} - E_i + V(r)q}{kT} \approx \exp\frac{E_{Fs} - E_i}{kT}, \tag{17}$$

$$\exp\frac{-(E_{Fs} - E_i) + V_{inj}(r)q}{kT} \approx \exp\frac{-(E_{Fs} - E_i)}{kT}. \tag{18}$$

We define $\sigma_s = \sqrt{\sigma_n\sigma_p}$, then Eq. (14) can be rewritten as

$$\frac{q\sigma_s v_{th} N_{it} n_i \{[V(r) + V_{inj}(r)]q/kT\}}{2[1 + \cosh(E_{Fs} - E_i^*)/kT]} = A^* T^2 \exp\left(\frac{-\Phi_B q}{kT}\right)\frac{V(r)q}{kT}. \tag{19}$$

It is useful to define the dimensionless ratio

$$M = \frac{q\sigma_s v_{th} N_{it} n_i}{2A^* T^2 \exp(-\Phi_B q/kT)[1 + \cosh(E_{Fs} - E_i^*)/kT]}. \tag{20}$$

Then Eq. (19) can be rewritten as

$$\frac{V_{inj}(r)q}{kT} = \frac{V(r)q}{kT}\left(\frac{1}{M} - 1\right), \tag{21}$$

which shows a linear relationship between $V(r)$ and $V_{inj}(r)$. M can be estimated for the Si(111)-7×7 surface. We find $M = 2.2 \times 10^{-3}$, using values $n_i = 10^{10}$ cm^{-3}, $A^* = 120$ A/cm^2 K^2, $T = 300$ K, $\Phi_B = 0.47$ eV, $k = 1.38 \times 10^{-23}$ J/K, $q = 1.6 \times 10^{-19} C$, $E_{Fs} = 0.65$ eV,[14] $E_i^* \approx E_i = 0.56$ eV, $v_{th} = 2.9 \times 10^7$ cm/s, $\sigma_s = (3.1$ Å$)^2$, and $N_{it} = 2.1 \times 10^{14}$ cm^{-2}.[15]

M has a simple physical meaning: for zero-bias condition, M is the ratio of surface R-G current density to thermionic emission current density on condition of no minority carrier injection. The fact that $M \ll 1$ indicates that high minority carrier injection level is necessary to keep the system in steady state (at any location, $J_{SB}=J_R$). This makes the Schottky point contact a minority carrier device.

Furthermore, substituting Eq. (21) into Eq. (12), we get $V_{inj}(r_0)=(1-M)V_0$ and $V(r_0)=MV_0$. With $M \ll 1$, we have $V(r_0) \approx MV_0 \ll V_0$, which means that only a small fraction of the applied bias drops along the surface. The small $V(r_0)$ limits the Ohmic surface current[16] due to a small potential drop along the surface and hence a small driving force, and it also limits the thermionic and tunneling currents for the point contact due to a strong "pinch-off" effect, as described by Ref. 7. So the Ohmic surface current, the thermionic current and tunneling current are all negligible, compared with the surface R-G current for this system. We note that the forms of $V(r)$ and $V_{inj}(r)$ have not been specified. These may be determined by considering the flow of minority carriers along the surface.

C. Minority carrier movement

In general, current flow includes both diffusion and drift components. For the point contact, drift current for minority carriers is small because $V(r_0)$ is small, as described above. Diffusion current, on the other hand, is large, due to minority carrier injection.

The minority carriers remain near the surface due to the built-in field, but they still extend into the space charge region. Hence, their transport is largely governed by bulk diffusion. This is characterized by the diffusion length L_D, which can be as large as 1 cm for bulk Si.[1] The diffusion length will be reduced by surface R-G and minority carrier injection, both of which are strongly dependent on the applied bias. For the moment, we assume a constant diffusion length. This assumption is valid in the zero-bias region. Then we have

$$\frac{\partial}{\partial r}\left[D_p\left(\frac{\partial p_s(r)}{\partial r}\right)\right]=\frac{p_s(r)-p_{s0}}{\tau}r, \tag{22}$$

which is the diffusion equation in cylindrical coordinates. Here, D_p is the diffusion coefficient for minority carriers (holes), p_{s0} is the minority carrier density at the surface under thermal equilibrium, and τ is the life time of minority carriers (holes).

The boundary conditions are the minority carrier density at r_0 and at infinity, which are denoted by $p_s(r_0)$ and $p_s(\infty)$ separately. At r_0, we have

$$p_s(r_0)=p_{s0}\exp\frac{V_{inj}(r_0)q}{kT}. \tag{23}$$

In the zero-bias region, Eq. (23) can be simplified as $p_s(r_0) \approx p_{s0}[1+(V_{inj}(r_0)q/kT)]=p_{s0}[1+(1-M)(V_oq/kT)]$. At infinity, we have

$$p_s(\infty)=p_{s0}. \tag{24}$$

Equation (22) has the form of Laplace's equation in cylindrical coordinates and can be solved analytically. The solution is

$$p_s(r)=p_{s0}\left[1+(1-M)\frac{V_0q}{kT}\frac{K_0(r/L_D)}{K_0(r_0/L_D)}\right], \tag{25}$$

in which $L_D=\sqrt{D_p\tau_p}$ and $K_0(r/L_D)$ is the modified Bessel function of the second kind. Furthermore, we have

$$V_{inj}(r)=(1-M)V_0\frac{K_0(r/L_D)}{K_0(r_0/L_D)} \tag{26}$$

and

$$V(r)=MV_0\frac{K_0(r/L_D)}{K_0(r_0/L_D)}. \tag{27}$$

The expressions for $V(r)$ and $V_{inj}(r)$ allow us to calculate the surface R-G current, and hence the zero-bias conduction. Substituting Eqs. (3), (4), (10), (11), (20), (26), and (27) into Eq. (2), we have

$$I_{\text{R-G}}=\frac{\pi q^2\sigma_s v_{th}N_{it}n_iV_0}{kT\left(1+\cosh\frac{E_{Fs}-E_i^*}{kT}\right)K_0\left(\frac{r_0}{L_D}\right)}\int_{r_0}^{\infty}rK_0\left(\frac{r}{L_D}\right)\mathrm{d}r. \tag{28}$$

The zero-bias conductance is then given by

$$G_0=\frac{I}{V_0}=\frac{\pi q^2\sigma_s v_{th}N_{it}n_i}{kT\left(1+\cosh\frac{E_{Fs}-E_i^*}{kT}\right)K_0\left(\frac{r_0}{L_D}\right)}\int_{r_0}^{\infty}rK_0\left(\frac{r}{L_D}\right)\mathrm{d}r. \tag{29}$$

III. CALCULATION AND COMPARISON WITH EXPERIMENT

The expression for zero-bias conductance derived from the model can be used to analyze the behavior of nanocontacts and to compare with experimental results.

A. Influence of the surface Fermi level on zero-bias conductance

Equation (29) shows a simple qualitative relationship between G_0 and E_{Fs} as

$$G_0 \propto \frac{1}{1+\cosh(E_{Fs}-E_i^*)/kT}, \tag{30}$$

which predicts a peak of G_0 for $E_{Fs}=E_i^*$, and an exponential decrease in G_0 as E_{Fs} moves away from E_i^*. The dramatic dependence of G_0 on E_{Fs} is a characteristic behavior of the surface R-G current and resembles the earlier reported experimental result for the point contact measurement on the Co-covered Si(111) surface, as shown in Fig. 3 and detailed discussed in Ref. 9. In this experiment, the surface Fermi level was adjusted by depositing Co onto Si(111)-7×7 at 650 °C, producing a "1×1 ring-cluster structure."[17,18] We assume that the surface Fermi level changes linearly with coverage from 0.65 eV at 0 ML to 0.42 eV at the saturation coverage of 1/7 ML.[14,19]

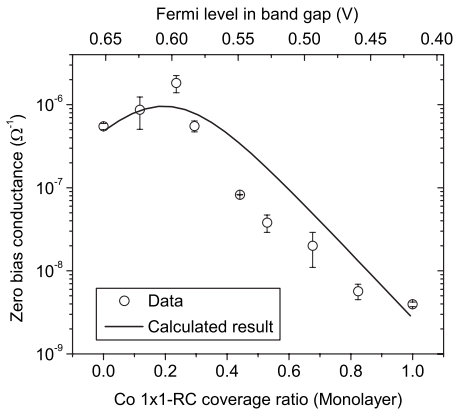

FIG. 3. Zero-bias conductance vs surface Fermi level (model) or Co coverage (experiment) for W point contact on Si(111).

A quantitative fit can be obtained, as shown in Fig. 3, by assuming $E_{Fs}=(1-\theta)E_{\mathrm{Si}}+\theta E_{\mathrm{Co}}$ (θ is the Co 1×1 coverage ratio), using values: $r_0=10$ nm, $N_{it}=2.1\times10^{14}$ cm^{-2}, $E_{\mathrm{Si}}=0.65$ eV and $E_{\mathrm{Co}}=0.42$ eV,[19] and adjusting the values of β and L_D in the model. From the fitting, we find that $E_i^*=0.61$ eV, $\sigma_p=35\sigma_n$ ($\beta=1/35$), and $L_D=38$ μm. We also note that the calculated curve deviates from the experimental result in the medium coverage range. This deviation might be ascribed to N_{it} which is assumed to be constant in the model but actually varies with Co coverage.

B. Influence of the contact area size on zero-bias conductance

In Fig. 4, we show the calculated and measured zero-bias conductance vs contact area, using Eq. (29) with parameters as above for clean and Co-covered surfaces. We use the saturated Co 1×1RC surface since the $CoSi_2$ islands are always surrounded by this structure. The calculated conductance for Si(111)-7×7 and Co 1×1RC are nearly constant at 5×10^{-7} Ω^{-1} and 3×10^{-9} Ω^{-1}, respectively. The measured conductance is nearly constant at 3×10^{-10} Ω^{-1}, independent of the contact size. The size independence agrees with the calculated trend, although the value is one magnitude lower. We believe this is due to imperfect injection of minority current from the island to the surface, which is caused by step bunches that surround the islands.[20] We have

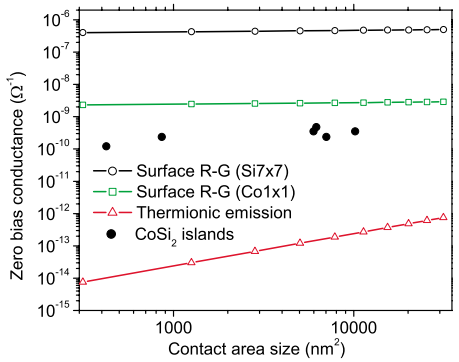

FIG. 4. (Color online) Calculated zero-bias conductance as a function of the contact area size for surface R-G current and for thermionic emission current, compared with the experimental results for $CoSi_2$ islands.

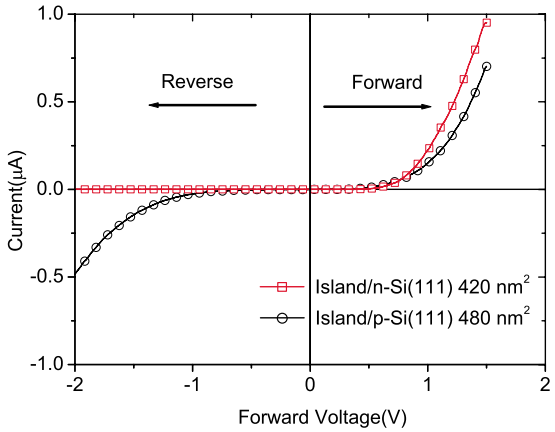

FIG. 5. (Color online) Measured I-V curves for n-type and p-type substrates, with similar doping and island size. The p-type substrate shows a soft breakdown under reverse bias.

included the calculated thermionic current, using Eq. (1) (ideal diode, with SBH=0.67 eV), and see that it is several magnitudes smaller than the measured conductance in this size range. We note that the thermionic current, which scales with contact size, will exceed the surface current for islands larger than $(1\ \mu\mathrm{m})^2$.

C. The nonzero-bias I-V curve

The discussion above focuses on the properties in the zero-bias region. In this section, we discuss qualitatively the I-V behavior in the whole bias range by investigating the variation in the surface R-G rate with bias, since the total current is dominated by this current.

We first consider the primary term, $n_sp_s-n_i^2$ in Eq. (4), which works as the driving force for the surface R-G current. Then we have

$$R_s \propto n_sp_s - n_i^2. \tag{31}$$

For large forward bias, $n_sp_s=n_i^2\exp[(Vq)/(kT)]\gg n_i^2$, so

$$R_s^{fwd} \propto n_i^2 \exp\frac{Vq}{kT}. \tag{32}$$

For large reverse bias, $n_sp_s\ll n_i^2$, so

$$R_s^{rev} \propto n_i^2. \tag{33}$$

Equations (32) and (33) clearly show that R_s increases exponentially with forward bias, and keeps constant under reverse bias. The R-G current behaves in the same manner, resulting in a rectifying I-V curve.

However, a surprising result exists for point contacts to p-type substrate, as shown in Fig. 5. In this figure, we show two typical I-V curves collected from similar-sized $CoSi_2$ islands which are grown on n-type and p-type Si substrates separately. Both substrates have similar doping level of 10^{15} cm^{-3}. For n-type substrate, the I-V curve shows a typical rectifying shape, while for p-type substrate, a soft breakdown occurs under reverse bias. This behavior can be well explained by the surface R-G process.

Next, we consider the secondary term, $\sigma_n[n_{1s}+n_s(r)]+\sigma_p[p_{1s}+p_s(r)]$ in Eq. (4), which can be simplified as n_s

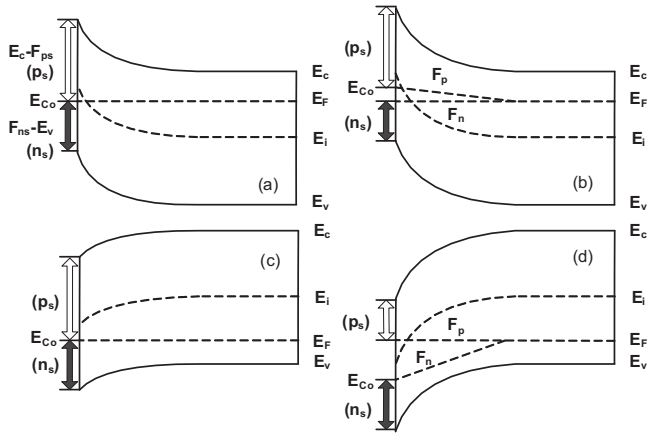

FIG. 6. Band bending for n-type and p-type Si surface under reverse bias voltage, (a) and (b) n-type Si, and (c) and (d) p-type Si.

$+p_s+2n_i$ with the assumption $\sigma_n=\sigma_p$ (so $p_{1s}=n_{1s}=n_i$). The influence of this term appears under reverse bias where the value of $n_s p_s - n_i^2$ is small. For large reverse bias, $p_s n_s \ll n_i^2$, so

$$R_s \approx \frac{\sigma_s v_{th} N_{it} n_i^2}{n_s + p_s + 2n_i}. \tag{34}$$

Thus, R_s mainly depends on $n_s+p_s+2n_i$, in which n_s and p_s are determined by F_{ns} and F_{ps} separately and can be schematically described with a band bending diagram. For example, for $CoSi_2$ islands on Si(111), the band bending diagram for n-type and p-type substrates at equilibrium are shown in Figs. 6(a) and 6(c), respectively. (It is found by STM imaging that the $CoSi_2$ islands are always surrounded by the Co 1×1RC surface, so the Fermi level of the surrounding surface is equal to E_{Co} which is 0.42 eV above the valence band maximum.) The magnitude of n_s depends on the separation between F_{ns} and the valence band maximum, as shown by the filled arrow in Fig. 6. The larger this separation, the larger n_s will be. And when the separation is equal to half of the band gap, that is, $F_{ns}=E_i$, we have $n_s=n_i$. The magnitude of p_s can be obtained in like fashion, as shown by the hollow arrow in Fig. 6.

Under zero-bias condition, both n-type and p-type substrates behave similarly, and we have $p_s \gg n_i \gg n_s$ and $n_s+p_s+2n_i \approx p_s$, as shown in Figs. 6(a) and 6(c). However, under large reverse bias, the behavior of n-type and p-type substrates are dramatically different. For n-type substrate, we have $F_{ps}=E_{Co}$ and $F_{ns}=E_F$, as shown in Fig. 6(b), resulting in an unchanged p_s and a decreased n_s. Thus, we find $n_s+p_s+2n_i \approx p_s$ and $R_s=\sigma_s v_{th} N_{it} n_i^2/p_s$, which shows that R_s is small and constant for reverse bias and indicates a typical rectifying I-V curve. For p-type substrate, we have $F_{ns}=E_{Co}$ and $F_{ps}=E_F$, as shown in Fig. 6(d), resulting in an unchanged n_s and a decreased p_s. For sufficiently large reverse bias, we have $p_s \ll n_i$, $n_s \ll n_i$, $n_s+p_s+2n_i \approx 2n_i$, and $R_s=\sigma_s v_{th} N_{it} n_i^2/(2n_i)$. We note that R_s increases significantly from $\sigma_s v_{th} N_{it} n_i^2/p_s$ for small reverse bias to $\sigma_s v_{th} N_{it} n_i^2/(2n_i)$ for large reverse bias, indicating relatively large current at large reverse bias. This causes a soft breakdown for large reverse bias and the condition for the soft breakdown can be simply obtained by comparing the two band bending diagrams, as shown in Fig. 5: the soft breakdown only occurs when E_F and E_i do not cross each other in the depletion region. Thus, we note the reverse current at large bias depends strongly on substrate doping type. The soft breakdown implied that, not just in the zero-bias range, the I-V behavior for nanoscale point contact is dominated by the surface R-G current in the whole bias range.

IV. CONCLUSION

We have developed an analytic model for the I-V behavior of a nanoscale Schottky contact, emphasizing the role of minority carriers and considering a full range of forward and reverse bias. The minority carriers give rise to a surface R-G current that can be much larger than the majority current across the interface. The model is validated by close comparison with measured I-V curves for nanoscale $CoSi_2$ or W contacts on Si(111). The dominant R-G current explains two nonideal features of nanoscale contacts including independence of zero-bias conductance on island size and soft reverse breakdown for p-type Si. The signature behavior for the R-G current is a strong variation in current with position of the surface Fermi level.

The analytic model developed here clearly reveals the underlying physics of the transport process. It may be solved in approximate form for near-zero bias. For large bias, a numerical solution would be required.

The minority current flow induced by surface R-G processes is generic to all nanoscale semiconductor contacts, though its magnitude and relative importance will depend on electrode geometry and surface recombination properties. Such effects can have dramatic influence on the transport properties of nanoscale electronics.

ACKNOWLEDGMENTS

This work was supported by NSF Grant No. DMR0503705.

[1] S. Sze and K. Ng, *Physics of Semiconductor Devices* (Wiley, Hoboken, New Jersey, 2006).
[2] F. Giannazzo, F. Roccaforte, F. Iucolano, V. Raineri, F. Ruffino, and M. G. Grimaldi, J. Vac. Sci. Technol. B **27**, 789 (2009).
[3] F. Ruffino, M. G. Grimaldi, F. Giannazzo, F. Roccaforte, and V. Raineri, Appl. Phys. Lett. **89**, 243113 (2006).
[4] M. Hugelmann and W. Schindler, Appl. Phys. Lett. **85**, 3608 (2004).
[5] G. D. J. Smit, S. Rogge, and T. M. Klapwijk, Appl. Phys. Lett. **80**, 2568 (2002).
[6] G. D. J. Smit, S. Rogge, and T. M. Klapwijk, Appl. Phys. Lett. **81**, 3852 (2002).
[7] T. Sato, S. Kasai, and H. Hasegawa, Appl. Surf. Sci. **175–176**, 181 (2001).
[8] U. Landman, R. Barnett, A. Scherbakov, and P. Avouris, Phys. Rev. Lett. **85**, 1958 (2000).
[9] L. Hao and P. A. Bennett, Nanotechnology **20**, 355201 (2009).
[10] W. Shockley, Phys. Rev. **87**, 835 (1952).
[11] D. J. Fitzgerald and A. S. Grove, Surf. Sci. **9**, 347 (1968).
[12] A. Many and D. Gerlich, Phys. Rev. **107**, 404 (1957).
[13] R. T. Tung Mater. Sci. Eng. R. **35**, 1 (2001).
[14] F. J. Himpsel, G. Hollinger, and R. A. Pollak, Phys. Rev. B **28**, 7014 (1983).
[15] J. Hsu, C. Bahr, A. Felde, S. Downey, G. Higashi, and M. Cardillo, J. Vac. Sci. Technol. A **10**, 985 (1992).

[16]Y. Hasegawa, I. W. Lyo, and P. Avouris, Surf. Sci. **357–358**, 32 (1996).
[17]P. A. Bennett, M. Copel, D. Cahill, J. Falta, and R. Tromp, Phys. Rev. Lett. **69**, 1224 (1992).
[18]P. A. Bennett, S. Parikh, M. Lee, and D. Cahill, Surf. Sci. **312**, 377 (1994).
[19]R. Flammini, F. Wiame, R. Belkhou, and A. Taleb-Ibrahimi, Appl. Surf. Sci. **233**, 411 (2004).
[20]F. Ross, P. A. Bennett, R. Tromp, J. Tersoff, and M. Reuter, Micron **30**, 21 (1999).